

## ANALYTICAL AND NUMERICAL MODELS OF SOUND RADIATION BY AIR-CORE REACTORS

**Thiago A. Fiorentin, thiago\_antonio@hotmail.com**

**Leonardo Ferreira Lopes, engleonardo@yahoo.com.br**

**Arcanjo Lenzi, arcanjo@emc.ufsc.br**

Federal University of Santa Catarina - UFSC

Department of Mechanical Engineering

Laboratory of Acoustics and Vibration

C.P. 476

88040-900 – Florianópolis - SC, Brazil

**Marlon Ferreira Arantes, marlon.arantes@areva-td.com**

**Daniel de Oliveira Lacerda, daniel.lacerda@areva-td.com**

AREVA T&D Brasil

Av. Nossa Sra. Da Piedade, 1021

37504-358 – Itajubá - MG, Brazil

**Abstract.** *The purpose of this paper is to provide an overview of the radiated sound power by air-core reactors, describing how the sound power level radiated by these electrical equipments can be calculated using the electrical load. Particularly, the sound power radiation of an air-core reactor is related to the alternating current harmonics, the mechanical tension stiffness and mainly the breathing mode resonance. Based on electrical the loads and mechanical properties of the air-core reactor, an analytical model is developed to calculate radial and axial forces caused by the radial and axial magnetic induction fields. The hemispherical spreading theory, a simple and common method to predict sound propagation was used. Additionally, a numerical model is proposed, in which the excitation of the acoustic field that surrounds the reactor is introduced by the consideration of the radial and axial displacements of the reactor's windings, since the windings are subjected to the action of the radial and axial electromagnetic forces. Finally, it is presented a comparison between analytical and numerical models that shows good agreement in the results obtained for reactor sound level pressure.*

**Keywords:** *Air-core reactors, high voltage direct current (HVDC) system, mechanism of sound generation, generated sound power, finite elements method, and numerical analysis.*

### 1. INTRODUCTION

When considering the impact of audible noise emanating from a high voltage direct current (HVDC) station, the alternating current (AC) filter reactors and the HVDC smoothing reactor are the main types of reactors which need to be considered. In this paper is described the mechanism of sound generation in air-core reactors. Two models for the calculation of the sound power level of the reactor are presented. The analytical model estimates the sound power from the radial and axial force created by the axial and radial magnetic field that acts over the reactor. The numerical model uses the radial and axial forces calculated by the analytical model as the excitation of the acoustic field that surrounds the reactor. The analytical and numerical results of a typical configuration of an air-core reactor used in HVDC system are presented and a comparison between them is made.

### 2. DESIGN OF AIR-CORE REACTORS AND MECHANISM OF SOUND GENERATION

It is common practice to employ air-core reactor technology for many applications in a high voltage direct current system. According to Clark M. et al., in an HVDC system, reactors are used for many functions. HVDC smoothing reactors connected with the HVDC transmission line and cable or inserted in the intermediate DC circuit of a back-to-back link are used to reduce the harmonics on the DC side, to reduce the current rise caused by failures in the DC system and to improve the dynamic stability in the HVDC system. Filter reactors are installed for harmonic filtering on the AC and on the DC side. Power line carrier and radio interference filter reactors employed on the AC and DC side of the HVDC station are used to reduce high frequency noise propagation in the lines. Shunt reactors may form part of an HVDC station to provide inductive compensation for AC harmonic filters, especially under light load conditions, where a certain minimum number of harmonic filters are required to satisfy harmonic performance requirements.

The major construction features of an air-core reactor are illustrated in Fig. 1. The winding of the reactor consists of one or multiple resin-impregnated and encapsulated winding layers made of insulated aluminium conductors. The concentric layers are connected in parallel by welding their ends to metallic beam structures (spiders). Both the top and bottom spider are clamped together by several sets of fiberglass ties located along the winding. The packages are radially spaced by circumferentially arranged fiberglass-reinforced sticks, which form vertical air ducts for natural convective cooling of the windings.

The noise generated by air-core reactors results mainly from vibration winding forces caused by the interaction of the current flowing through the winding and its magnetic field. The forces in the winding are proportional to the current multiplied by the magnetic field in the winding, and thus they are proportional to the square of the current. From the sound generating point of view the forces of interest are primarily those in radial direction, since they create vibrations on the surface which can create propagating sound waves in the air (Smede J. et al, 1995).

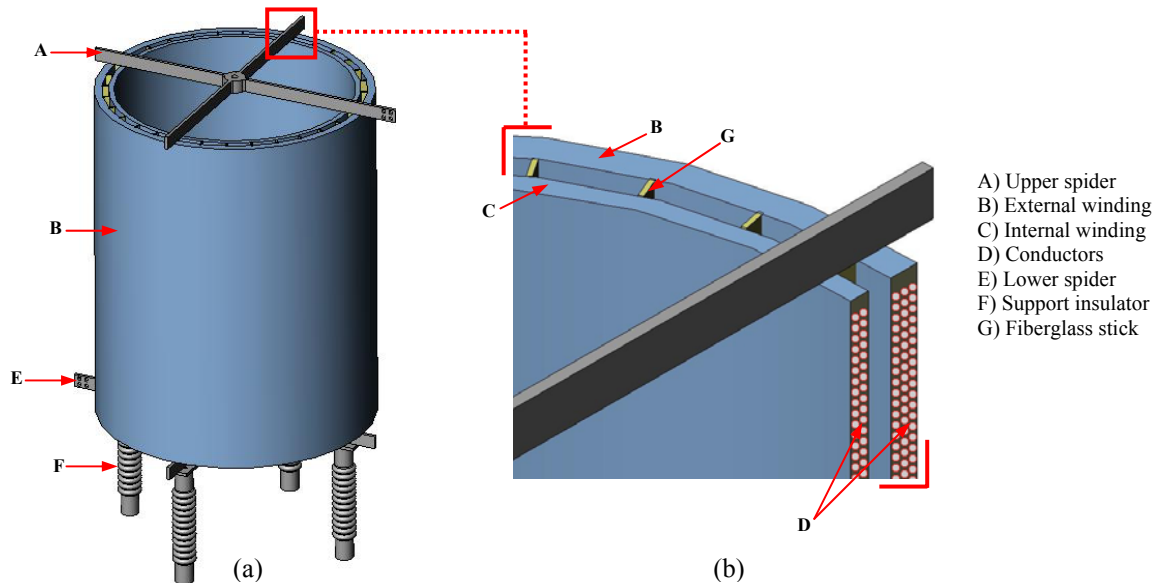


Figure 1. Air-core reactor: (a) General view, (b) Section view.

The acoustic frequency spectrum depends on the load current spectrum of the reactor, and is thus very much dependent on the reactor application. In case of single frequency AC current, the forces are oscillating with twice the frequency of the current. If, however, the reactor is simultaneously loaded by several currents of different frequencies, in addition to vibration modes at double the electrical frequencies there also additional vibration frequencies. The last situation is better illustrated by the simplified current spectrum of an AC filter reactor, Figure 2 (a), in which the current consists of a component with fundamental frequency  $f$  and one harmonic component with harmonic order,  $h$ . The force acting on the winding of these reactor consists of a static pre-load and components with frequencies  $2f$ ,  $f(h-1)$ ,  $f(h+1)$  and  $2fh$ , as is shown at Figure 2 (b). Only the vibration force components are generating noise; the static pre-load does not affect the sound power.

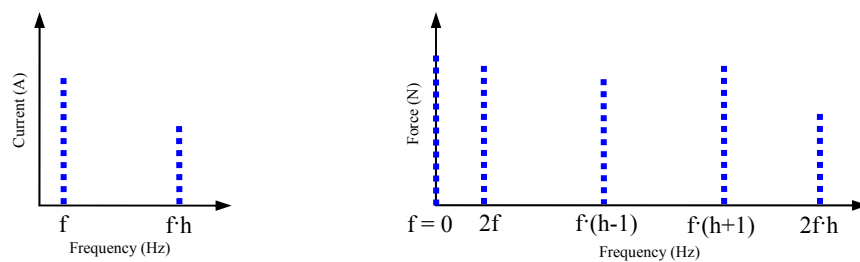


Figure 2. Example of spectrum: (a) Currents through AC filter reactor, (b) Forces acting on the reactor winding.

So it may be concluded that when going from electrical load to electrical force, a frequency shift occurs and the number of force components is equal to the square of the number of load components. The acoustic frequency spectrum will therefore increase significantly if the reactor current spectrum includes several harmonics.

As any mechanical structure, the dynamic behaviour of the reactor may be described in terms of vibration modes caused by these electromagnetic forces. Since the oscillating forces are of almost rotational symmetry, it would be expected that only symmetrical modes of the structure coinciding with the shape of the force distribution would be excited. However, the finite number of duct sticks between concentric windings, the spiders attached at the winding ends and manufacturing tolerances result in the excitation of modes other than those of rotational symmetry. The fundamental modes of the cylindrical reactor structure are:

a) The “breathing mode”: in this mode the forces are uniformly distributed around the reactor and try alternately to expand and compress the winding in the radial direction, or in other words, the reactor winding is deformed as a cylindrical pressure vessel. This modal frequency essentially depends on the material parameters of the winding and is inversely proportional to the winding diameter. The breathing mode is fully symmetrical and its shape coincides with the distributed exciting electromagnetic force resulting from the axial magnetic field component.

b) The “compression mode” in the axial direction where the reactor is symmetrically compressed towards the reactor midplane. This mode is excited by the radial magnetic field component.

c) The “flexural modes” (bending modes) of the winding layers, characterized by the number of nodes in circumferential and axial direction. The frequencies of interest for these modes are usually lower than the breathing mode frequency. Although the flexural modes are not of rotational symmetry they become excited by the electromagnetic forces.

The vibration amplitude and size of the sound radiating surface of the apparatus essentially determine the sound power. Therefore, the sound emission of an air-core reactor is governed by the magnitude of the winding vibration in the radial direction, since the winding represents the main part of the radiating surface. The contribution of axial winding vibrations and that of other components to the total sound emitted is relatively low.

In this paper are presented the results of an air-core reactor, which has the configuration usually found in HVDC stations. It has one winding and natural cooling. Its winding is formed by four layers of insulated aluminium conductors. Among the conductors there are layers of fiberglass with epoxy resin. The other geometrical characteristics of the reactor are showed in Table 1.

To develop the analytical model of radiation, the structure of each turn of the reactor is simplified to an equivalent turn that has the same area of the original one. In Figure 3 (a) and (b) can be observed, respectively, the original and the equivalent structure of one turn.

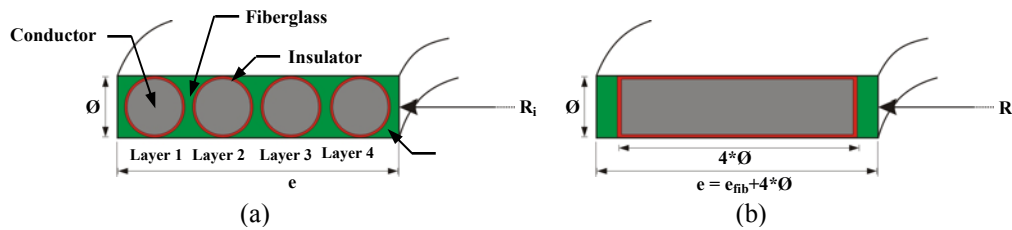


Figure 3. Structure of each turn of the reactor: (a) Original, (b) Equivalent.

Table 1. Geometrical characteristics of the reactor.

Geometrical characteristics of the reactor	Nomination	Values
Diameter of the conductor without insulating	$\varnothing_{ni}$	3.80E-03 m
Diameter of the insulated conductor	$\varnothing$	4.20E-03 m
Average height of the winding	$H$	1.448 m
Distance between turns (centre to centre)	$d$	4.20E-03 m
Internal radius of the winding	$R_i$	0.60 m
External radius of the winding	$R_e$	0.62 m
Average radius of the winding	$R$	0.61 m
Mass of the winding	$M$	290 kg
Thickness of the winding	$e$	2.04E-02 m
Thickness of the insulation	$e_{iso}$	4.00E-04 m
Thickness of the fiberglass layer	$e_{fib}$	3.60E-03 m
Total average number of turns in the winding	$nbr$	345 turns

### 3. ANALYTICAL MODEL

Alternating currents through the reactor produce simultaneously an electric field (due to the electric charges) and a magnetic field (due to the flowing current). The resulting electromagnetic interaction involves the creation of an electromagnetic force which causes the vibration of the walls. The determination of the expression of the magnetic induction field in all points of the winding involves the solution of complex numerical equations which does not enable to obtain a simple analytical expression of the field according to the parameters of the system. Therefore, to develop an analytical model some hypothesis are assumed and the magnetic induction field is broke up in two parts: the radial magnetic induction field ( $B_{radial}$ ) and the axial magnetic induction field ( $B_{axial}$ ). This form will allow the division of the problem in two parts: the radial mode involves the calculation of the axial field, which causes a radial electromagnetic force ( $F_{radial}$ ). And the axial mode, that involves the calculation of the radial field which causes an axial electromagnetic force ( $F_{axial}$ ).

The determination of the expressions of the radial and axial field will be carried out by the use of the following relations:

a) The Law of Biot and Savart expresses the value of the magnetic induction field  $\mathbf{B}$  created by an infinitesimal element of current  $d\mathbf{l}$  in a distant point  $r$  of the source.

$$\mathbf{B}(t) = \frac{\mu_0}{4\pi} i(t) \oint \frac{d\mathbf{l} \times \mathbf{r}_0}{r^3} \quad (1)$$

The constant of proportionality,  $\mu_0$ , is the permeability of free space. The small circle on the integral sign indicates that the path of integration is a closed loop. Admitting that the current has a sinusoidal behavior in respect to time, it can be defined by expression:

$$i(t) = \sqrt{2} I_{eff} \sin(\omega t) \quad (2)$$

where,  $I_{eff}$  is the effective current (A) and  $\omega$  is angular frequency of the current (rad/s).

b) Ampere's Law provides a method for evaluating  $\mathbf{B}$  fields when the current distribution has some simplifying features. The law relates the path integral of the magnetic induction field  $\mathbf{B}$  round a closed loop to the total current  $i(t)$  passing through the loop. In mathematical terms this can be written:

$$\oint \mathbf{B}(t) d\mathbf{l} = \mu_0 i(t) \quad (3)$$

c) The electromagnetic force expresses the electromagnetic force  $\mathbf{F}$  undergone to the conductor of length  $d\mathbf{l}$  caused by a current and subjected by a magnetic induction.

$$\mathbf{F}(t) = \oint i(t) d\mathbf{l} \times \mathbf{B}$$

### 3.1. Radial mode

To simplify the development of equations, the value of the axial induction field is calculated on the axis of the winding, as illustrated in Fig. 4. This one will be supposed uniformly distributed into the winding and on the conductors. According to Grégory P. (1998) the magnetic induction field in a point P of the axis of the winding, Eq. (4), can be estimated by the initial calculation of the field on the axis of one turn using the Law of the Biot and Savart followed by the extrapolation of the expression to an assembly of n turns.

$$B(z, t) = \frac{\sqrt{2} \mu_0 I_{eff} N}{2} \left( \frac{z}{(R^2 + z^2)^{1/2}} + \frac{(H - z)}{(R^2 + (H - z)^2)^{1/2}} \right) \sin(\omega t) \quad (4)$$

where,  $\mu_0$  is the permeability of free space,  $I_{eff}$  is the effective current,  $N$  is the number of turns per unit of length ( $N = l/\varnothing$ ),  $z$  is the distance in Z axis of the point P,  $R$  is the average radius of the winding,  $H$  is the height of the winding ( $H = nbr \cdot \varnothing$ ), and  $\omega$  is the angular frequency of the current.

Observe that the axial induction field is maximum in the centre of the winding and minimum at two ends.

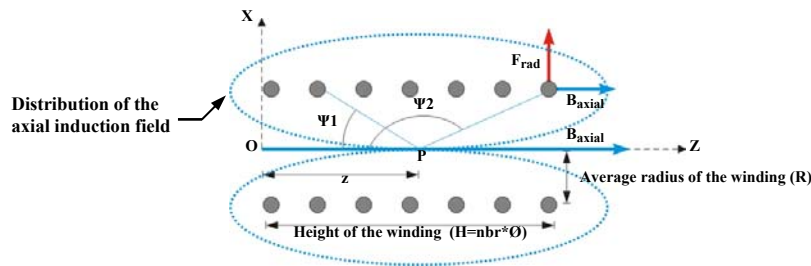


Figure 4. Axial induction field in a point P of the axis of the winding.

To avoid the complex integration of the Eq. (4) over the height of the winding, in the following calculations the expression of the average axial magnetic induction field, Eq. (5) will be used.

$$B_{axial}(t) = B_{avg,z}(t) = \frac{\sqrt{2} \mu_0 I_{eff} N}{H} \left( \left( R^2 + (H)^2 \right)^{1/2} - R \right) \sin(\omega t) \quad (5)$$

Because the turns of the winding are subjected to the average magnetic induction field  $B_{axial}$  (constant in all inner points of the winding), each turn of the winding is subjected to the same radial linear force  $F_{radial}$  determined by Eq. (7).

$$F_{radial}(t) = F_{avg,x}(t) = \frac{2\mu_0 I_{eff}^2 N}{H} \left( (R^2 + (H)^2)^{1/2} - R \right) \sin^2(\omega t) \quad (6)$$

The radial force is expressed in N/m and has the following properties:

- The force is unidirectional and repulsive (no deformation towards the inner part of the winding).
- The force is proportional to the square of the current ( $I_{eff}$ ) and proportional to the number of turns per unit of length ( $N$ ).
- The frequency of the average force is twice the frequency of the current.

In Fig. 5 is shown the distribution of the radial force acting over one turn of the winding.  $F_N$  is the normal force of traction that acts over the thickness of the turn. It is expressed in N.

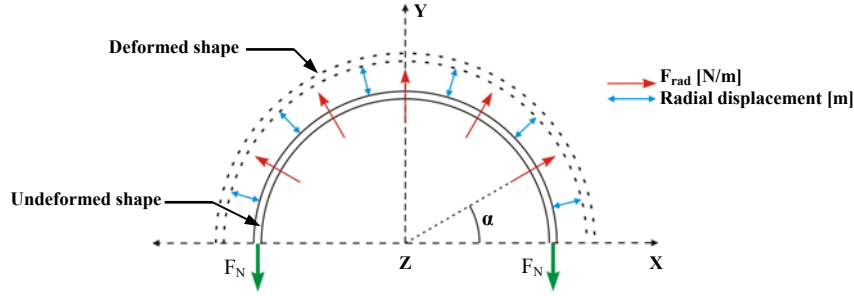


Figure 5. Radial displacement caused by the action of the radial force.

Making the vertical balance of the forces that act in Y direction, it can be possible to obtain the following equation for the radial displacement of the winding:

$$\Delta R(t) = \frac{2\mu_0 I_{eff}^2 R^2}{nbrEe\phi^3} \left[ (R^2 + (nbr\phi)^2)^{0.5} - R \right] \sin^2(\omega t) \quad (7)$$

where,  $nbr$  is the total average number of turns in the winding,  $\phi$  is the conductor diameter,  $e$  is the thickness of the winding,  $E$  is an equivalent young modulus calculated based on the total area of the winding undergone to the normal force, and the total areas of the conductor and fiberglass. The young modulus of the aluminium and the fiberglass are  $7.2E+10$  N/m<sup>2</sup> and  $3.0E+10$  N/m<sup>2</sup>, respectively.

Deriving the expression of radial displacement in respect to time will obtain the expression of the average radial speed of the winding:

$$v_{rad}(t) = \frac{4\mu_0 I_{eff}^2 R^2 \pi f}{nbrEe\phi^3} \left[ (R^2 + (nbr\phi)^2)^{0.5} - R \right] \sin(2\omega t) \quad (8)$$

where,  $f$  is the frequency of the current in Hz.

### 3.2. Axial mode

Supposing that the winding is formed by four turns located parallel one against other, as is shown in Fig. 6.

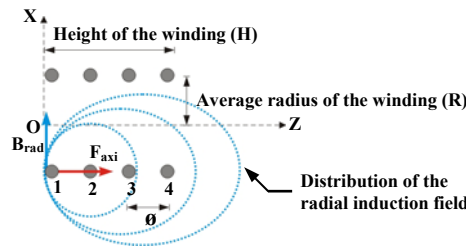


Figure 6. Radial induction field of the first turn of the winding<sup>1</sup>.

<sup>1</sup> For the comprehension of the drawing the turns were isolated, but actually the distance between them is null.

The radial induction field that acts over the first turn is equivalent to the sum of the contributions of the fields created by the others ones. In the other hand, the field that acts over the second turn is null because the cancellation of the induction of the first and third turn. So, it is possible concludes that the resulting field that acts over the median turn is null. Using these conclusions and the Ampere's Law for a linear conductor it may be obtained the radial induction field in a point located at  $z=0$ ,  $z<H/2$ ,  $z=H/2$ ,  $z>H/2$  and  $z=H$ . These expressions utilize convergent series that have hard solutions. For these reason, to simplify the analytical calculation procedure, these expressions are reduced to an expression that can be integrated on the half-height of the winding in order to obtain the average value of the radial magnetic induction field on both sides of the winding (Grégory P., 1998).

$$B_{radial}(t) = B_{avg,x}(t) = \pm \frac{\sqrt{2}\mu_0 I_{eff}}{4\pi\phi} \ln(nbr) \sin(\omega t) \rightarrow (+) \text{ when } z<H/2 \text{ and } (-) \text{ when } z>H/2 \quad (9)$$

$$B_{radial}(t) = B_{avg,x}(t) = 0 \rightarrow z=H/2 \quad (10)$$

where,  $\phi$  is the diameter of the conductor and  $nbr$  is the total average number of the turns in the winding.

Therefore, consider again that the winding is subject to average radial induction field. Each turn undergoes the same linear force:

$$F_{axial}(t) = F_{Z,média}(t) = \pm \frac{\mu_0 I_{eff}^2}{2\pi\phi} \ln(nbr) \sin^2(\omega t) \rightarrow (+) \text{ when } z<H/2 \text{ and } (-) \text{ when } z>H/2 \quad (11)$$

$$F_{axial}(t) = F_{Z,média}(t) = 0 \rightarrow z=H/2 \quad (12)$$

The axial force is expressed in N/m and has the following properties:

- The force is proportional to the square of the current ( $I_{eff}$ ).
- The frequency of the average force is twice the frequency of the current.
- The distribution of the axial force compresses the winding.

The axial force compresses the winding, therefore in this mode of deformation the winding can be seen as an assembly of system mass-spring-mass-spring, shown in Fig. 7 (a). The first mass consists of the sum of the mass of the conductor and fiberglass while the second mass corresponds to the sum of the mass of the insulator and fiberglass.

The general expression that defines the stiffness  $K$  of a mechanical system is:

$$K = \frac{ES}{l} \quad (13)$$

In this case,  $l$  corresponds to the height of the material,  $S$  indicates the surface of contact between two materials and  $E$  is the young modulus of the material. For one turn there will be the following stiffness:  $K_{Al}$ ,  $K_{fib1}$ ,  $K_{iso}$  and  $K_{fib2}$ .

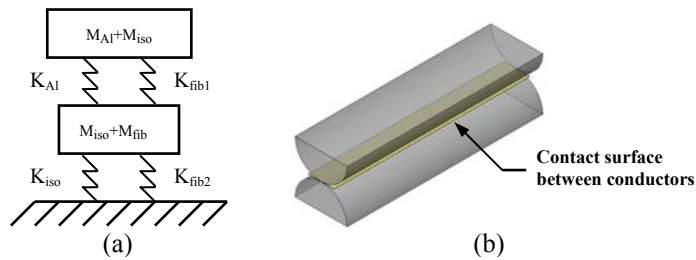


Figure 7. (a) Equivalent stiffness of each turn that form the winding (b) Contact surface between materials.

The surface of contact between conductor-insulator being weaker than the surface of contact fiberglass-fiberglass, so the stiffness  $K_{Al}$  and  $K_{iso}$  can be neglected when compared to respectively the stiffness  $K_{fib1}$  and  $K_{fib2}$ . Once the two springs are in series, the equivalent stiffness of the system is:

$$K_{eq} = \frac{K_{fib1}K_{fib2}}{K_{fib1} + K_{fib2}} \quad (14)$$

The young modulus of the material that form the turn can be obtained substituting the expression of the equivalent stiffness in Eq. (13), and considering that  $l$  is equal to the diameter of the turn.

$$E = \frac{K_{eq}\phi}{2\pi Re} \quad (15)$$

It may be observed that the value of the young modulus for the radial mode and axial mode are different.

As in radial mode, using the definition for the young modulus the expression for the axial displacement of the winding  $\Delta H$  can be obtained.

$$\Delta H(t) = \frac{\mu_0 I_{eff}^2 nbr}{2\pi E_{fib} e_{fib}} \ln(nbr) \sin^2(\omega t) \quad (16)$$

where,  $E_{fib}$  and  $e_{fib}$  is, respectively, the young modulus and the thickness of the fiberglass.

Deriving the expression of the axial displacement in respect to time will obtain the expression of the average axial speed of the winding:

$$v_{axi}(t) = \frac{\mu_0 f I_{eff}^2 nbr}{E_{fib} e_{fib}} \ln(nbr) \sin(2\omega t) \quad (17)$$

### 3.2. Acoustic model

According Blackstock (2000), the equation that defines the radiated sound power is:

$$W = \rho_0 c_0 S_W \sigma \langle \bar{v} \rangle^2 \quad (18)$$

where,  $W$  is the radiated sound power (W),  $\rho_0$  is the density of the air ( $\text{kg/m}^3$ ),  $c_0$  is the speed of sound in air (m/s),  $S_W$  is the sound radiating surface ( $\text{m}^2$ ),  $\sigma$  is the radiation efficiency and  $v$  is the RMS value of the vibration velocity (m/s) over the surface ( $\langle \rangle$ ) and time ( $\bar{\phantom{x}}$ ).

For the reactor, in radial direction the internal and external surfaces are responsible for sound generation ( $S_{Wrad} = 4\pi HR$ ), in the other hand, in axial direction the surface responsible for radiation is the cross sectional area of the winding ( $S_{Waxi} = e2\pi R$ ). The radiation efficiency depends on the frequency, geometrical and structural properties of the component, so the value establish for the radiation efficiency is multiplied by an correction factor to take account all approximations made on the analytical model (neglected internal deformation, dissipation...).

Using the considerations above, the radial and axial sound power of the winding are respectively, Eq. (19) and Eq. (20).

$$W_{rad} = 32 \rho_0 c_0 \pi^3 \mu_0^2 \sigma \frac{I_{eff}^4 R^5 f^2}{E^2 e^2 \phi^5 nbr} \left[ \left( R^2 + (nbr\phi)^2 \right)^{0.5} - R \right]^2 \quad (19)$$

$$W_{axi} = \rho_0 c_0 \pi \mu_0^2 \sigma \frac{f^2 I_{eff}^4 nbr^2 R}{E_{fib}^2 e_{fib}^2} [\ln(nbr)]^2 (e_{fib} + 4\phi) \quad (20)$$

Therefore, the sound level pressure generated by the reactor in dB can be expressed by the following expression:

$$L_W = 10 \log_{10} \left( \frac{W_{rad} + W_{axi}}{10^{-12}} \right) \quad (21)$$

The acoustic pressure emitted by the winding in a specific point where the receiver is founded depends on the comparison between the coordinates of the receiver and the dimension of the source. Indeed when the distance source-receiver  $r$  is large compared to dimensions of the source ( $r/H > 10$ ) the reactor is compared with a spherical source. As in the most of times the reactor is installed near the ground, the sound waves are reflected by the ground<sup>2</sup>, therefore the reactor is comparable with a half-spherical source. Add to that, for these distances, the acoustic energy of internal surfaces and the power of axial mode take part into acoustic pressure equation:

$$P = \sqrt{\frac{\rho_0 c_0 (W_{rad} + W_{axi})}{2\pi r^2}} \quad (22)$$

<sup>2</sup> It is supposed that the ground is a perfectly reflective surface, without absorption.

where,  $r$  is the distance from the receptor to the center of the winding.

In the other hand, when  $r/H < 10$  the reactor is comparable with a cylindrical source. At such distances, the participation of the noise generated by the interior wall can be neglected in front of that coming from external surface. The level of noise created by the axial mode may be also neglected, since its direction is parallel to the axis of the reactor.

$$P = \sqrt{\frac{\rho_0 c_0 W_{rad}}{4\pi(r + R_e)H}} \quad (23)$$

where,  $R_e$  is the external radius of the winding.

#### 4. NUMERICAL MODELS

The numerical models are developed using the finite elements method. The first step of the numeric modelling was to build the geometry corresponding to the reactor analyzed in our research and mesh it. The mesh used for the structural analysis was constructed using software Ansys 10.0®. The type of the element used was shell 63. This element is defined by four nodes, four thicknesses, an elastic foundation stiffness and the orthotropic material properties. Add to that, the element has both bending and membrane capabilities. Both in-plane and normal loads are permitted. The element has six degrees of freedom at each node: translations in the nodal x, y, and z directions and rotations about the nodal x, y, and z-axes.

According to the interest frequency, the mesh was divided in 18 elements in circumferential direction, and 8 elements in axial direction. The analytical forces  $F_{axi}$  and  $F_{rad}$  calculated by analytical model were used as boundary condition of the structural numerical model. The axial force multiplied by half height of the reactor was applied in the upper and lower nodes. The radial force was decomposed into x and y components and applied in all nodes of the model. The boundary conditions applied on the model are shown in Fig. 8.

The mechanical properties defined for the structural model were: Young modulus of the fiberglass (30 GPa) for axial and radial directions, and the young modulus calculated in the analytical model (58.9 GPa) for circumferential direction. Shear modulus  $G_{xy}$  equals that of the aluminium (26.7 GPa) and  $G_{xz}=G_{yz}$  determined experimentally (1.56 GPa). Poisson's ratio  $\nu_{xy}$  equals to that of the aluminium (0.25),  $\nu_{xz}=\nu_{yz}$  the same as the fiberglass (0.034). For density was used an average value calculated based on the area occupied by the aluminium and the fiberglass in respect to the total area of the reactor (2362 kg/m<sup>3</sup>).

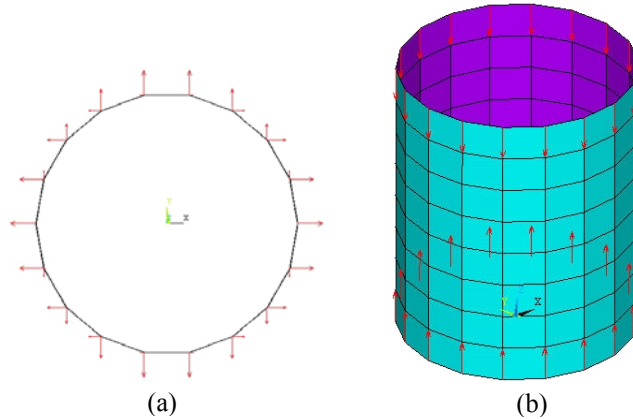


Figure 8. Boundary conditions: (a) Radial force decomposed into x and y directions (b) Axial force.

Using a harmonic solution the software Ansys® enables to calculate, for the interest frequency, the displacement of each node caused by the action of the axial and radial forces. These displacements were necessary to calculate the sound level pressure generated by the reactor, as will be explicated below, in the acoustic model.

The acoustic numeric model was developed to calculate the sound level pressure radiated by the reactor in a point located 500 mm of its external surface. The equivalent mesh created to represents this acoustic field has the same height of the reactor. The element type utilized was solid hexahedron with 8 nodes. The mesh discretization was the same that in the structural model, except in radial direction, which was divided in 3 elements, as is shown in Fig. 9 (a).

The impedance of the infinite medium  $\rho_0 c_0$  was used as boundary condition of all external surfaces in order to represents the free field that surrounding the reactor. The displacements on nodes calculated in earlier step were used as excitation of the acoustic field. In the software this boundary condition was made by the insertion of a vibrant panel in the interior surface of the mesh. These two boundary conditions applied in the acoustic numeric model can be observed at Fig. 9 (b) and (c).

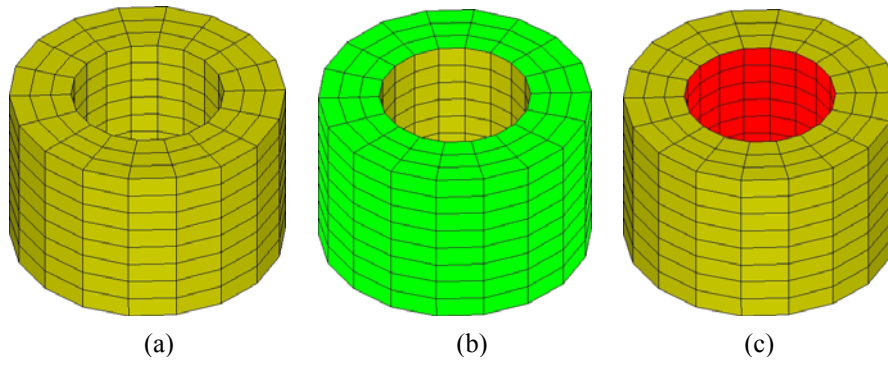


Figure 9. Mesh of the acoustic field: (a) Without boundary condition (b) Impedance of free field (c) Vibrant panel.

The numerical analysis was made using the software LMS Sysnoise 5.6®. The numeric solution enables to determine the sound level pressure in all nodes of the mesh.

## 5. COMPARISON BETWEEN ANALYTICAL AND NUMERICAL RESULTS

In this section is compared the analytical and numerical results obtained from an air-core reactor, which has the characteristics described in first section. For the calculations it is supposed that the reactor is loaded with a single AC current of 100 A and frequency of 130 Hz.

Consider the comparison between the frequency of the breathing mode, and 1<sup>st</sup> axial mode of the reactor. For the numerical model the 1<sup>st</sup> axial mode occurs at 1166 Hz while the breathing mode occurs at 1402.5 Hz. The nodal displacement vector sum and mode shape of each them can be observed in Fig 10.

The resonance frequency of the 1<sup>st</sup> axial mode of the reactor can be calculated analytically assuming that its behaviour is the same of a clamped-free bar. According to Inman (1996) the following equation is used for the determination of the 1<sup>st</sup> natural frequency of a clamped-free bar:

$$f_{axi} = \frac{1}{4} \sqrt{\frac{EV}{MH^2}} \quad (24)$$

where,  $V$  and  $M$  is, respectively, the volume total and mass total of the reactor.  $E$  is the young modulus in axial direction. The young modulus in axial direction was not determined, but it can assume the value of fiberglass young modulus or aluminium young modulus. Thus, in the analytical model it is possible conclude that the frequency of the 1<sup>st</sup> axial mode will be between these two extremes, 915 Hz (using young modulus of the aluminium) and 591 Hz (using young modulus of the fiberglass).

Analytically, in radial direction is assumed that the reactor has the behaviour of a linear mechanical system with one degree of freedom and without damping, so the resonance frequency can be calculated by the following equation:

$$f_{rad} = \frac{1}{2\pi} \sqrt{\frac{K}{M}} = \frac{1}{2\pi} \sqrt{\frac{Ee\phi nbr}{2\pi RM}} \quad (25)$$

where,  $E$  is the young modulus calculated for the radial mode. The substitution of each variable, in equation above, by their respective values enables to obtain the radial resonance frequency of 1252 Hz.

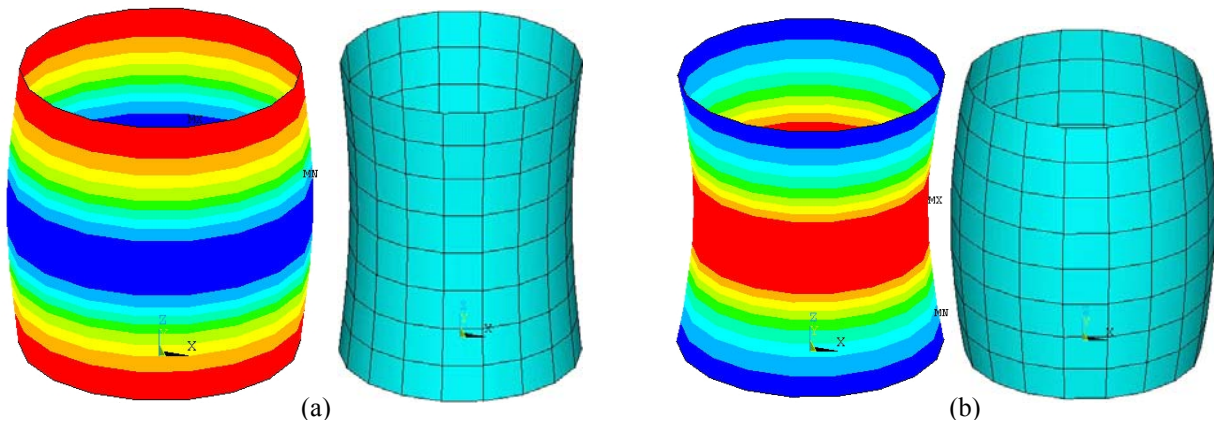


Figure 10. Nodal displacement vector sum and mode shapes: (a) 1<sup>st</sup> axial mode, (b) Breathing mode.

The distribution of sound levels pressure calculated by numeric model is showed in Fig. 11. Hot colours indicate higher pressure levels. In the internal surface of the mesh, which one is coincident with the external reactor's surface are registered the highest levels pressure, 57.4 dB. In external mesh surface the higher sound levels pressure are 54 dB, located in the middle of the mesh.

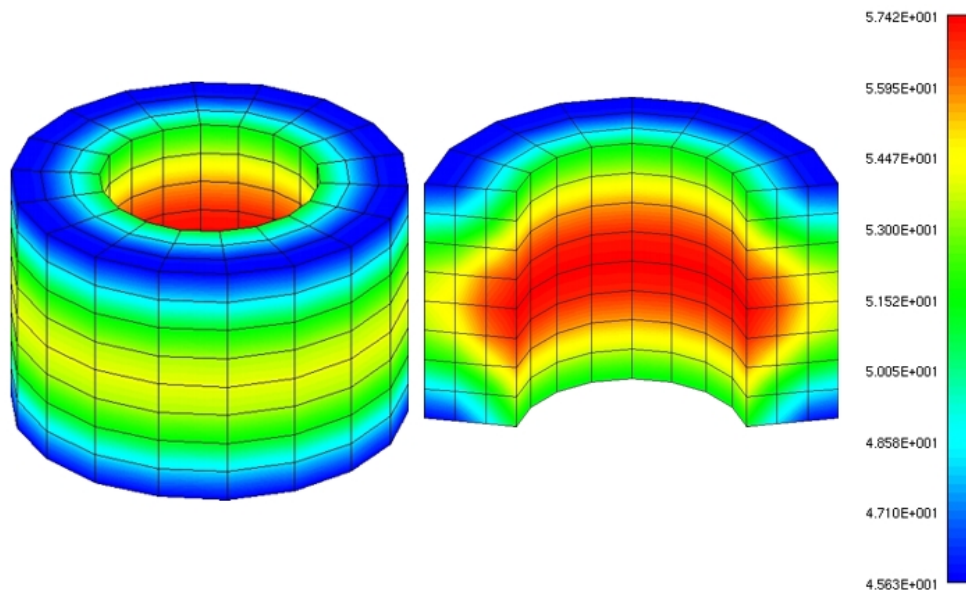


Figure 11. Sound level pressure in the acoustic field that surrounding the reactor.

The average sound level pressure calculated with the analytical model for a point located in the external surface of the reactor and for a point far 500 mm from the external surface are respectively, 59.7 dB and 56.8 dB. Add to that, the sound power level caused by the radial mode is 75.4 dB while that caused by axial mode is 36.0 dB, confirming that the breathing mode has the major contribution for the sound radiation of the reactor.

## 6. CONCLUSIONS

The comparison between analytical and numerical results for the radial and 1<sup>st</sup> axial resonances of the reactor presents some differences. They can be explicated for the simplification and hypotheses assumed in analytical model to calculate these resonance frequencies.

In the other hand, the results of the sound level pressure show good agreement, demonstrating that the analytical model can be useful to calculate the sound pressure generated by air-core reactors. Additionally, the analysis of the radial and axial sound power levels proves the great contribution of the breathing mode in the acoustic energy radiated by the reactor.

## 7. REFERENCES

- Blackstock, D.T.,2000, "Fundamentals Of Physical Acoustics", Ed. John Wiley & Sons, Inc., New York, USA, 541p.
- Clark, M., et al., "WG 14.26-HVDC Stations Audible Noise", Report of International Council on Large Electric Systems - CIGRE, pp. 01-99.
- Grégory P., 1998, "Réactances de Compensation: Vibrations et gêne Acoustique"(In french). 1998. Final Academic Report, University of Liège, Belgium.
- Inman, D.J.,1996, "Engineering Vibration", Ed. Prentice-Hall, Inc., Englewood Cliffs, New Jersey, USA, 560p.
- Smede J., et al., 1995, "Design of HVDC Converter Stations With respect To Audible Noise Requirements", IEEE Transactions on Power Delivery, Vol. 10, No. 2, pp. 747-758.

## 5. RESPONSIBILITY NOTICE

The authors are the only responsible for the printed material included in this paper.